Barrier-free microfluidic paper analytical devices for multiplex colorimetric detection of analytes

Ayushi Chauhan, Bhushan J. Toley*

Department of Chemical Engineering
Indian Institute of Science
Bangalore, India

*Correspondence to:
Bhushan J. Toley
Department of Chemical Engineering
Indian Institute of Science Bangalore
Malleswaram
Bangalore 560012
Phone: +91-9146142296
Email: bhushan@iisc.ac.in

Abstract

In recent years, microfluidic paper analytical devices (μPADs) have been extensively utilized to conduct multiplex colorimetric assays. Despite their simple and user-friendly operation, the need for patterning paper with wax or other physical barriers to create flow channels makes large scale manufacturing cumbersome. Moreover, convection of rehydrated reagents in the test zones leads to non-uniform colorimetric signals, which makes quantification challenging. To overcome these challenges, we present a new device design called barrier-free μPAD (BF-μPAD) that consists of a stack of two paper membranes having different wicking rates – the top layer acting as a fluid distributing layer and the bottom layer containing reagents for colorimetric detection. Multiple analytes can be detected using this assembly without the need to pattern either layer with wax or other barriers. In one embodiment, a device is capable of delivering the sample fluid to 20 distinct dried reagent spots stored on an 8cm x 2cm membrane in as few as 30 seconds. The multiplexing feature of BF-μPAD is demonstrated for colorimetric detection of salivary thiocyanate, protein, glucose, and nitrite. Most importantly, the device improves the limit of detection of colorimetric assays performed on conventional μPADs by more than 3.5x. To understand fluid imbibition in the paper assembly, the device geometry is modelled in COMSOL Multiphysics using Richards equation; the results obtained provide insights into the non-intuitive flow pattern producing perfectly uniform signals in the barrier-free assembly.

Introduction

Microfluidic paper analytical devices (µPADs) have become a powerful tool for point-of-care (POC) diagnosis owing to their portability, user-friendliness, biodegradability, compatibility with biological fluids, and the ability to store dried reagents[1]. One of the most popular applications of µPADs has been the multiplexed colorimetric detection of analytes in a sample fluid[1,2]. Detection of multiple analytes is performed by patterning hydrophobic barriers on the membrane to create flow channels, a technique first demonstrated by Martinez et al.[3] Multiple techniques have since been utilized for the creation of such barriers, e.g. wax printing, inkjet printing, photolithography, chemical modification of paper etc.; these techniques have been well reviewed by Cate et al.[2]

Despite their popularity, the techniques used for patterning paper require specialized equipment that increase the cost of fabrication. Further, each technique has associated limitations, e.g. low print resolution in wax printing and inkjet printing, and the need for a clean room, UV exposure facility, and skilled personnel for photolithography techniques. An alternative to patterning is to precisely cut the paper membrane in the desired shape[4]. But this method limits the smallest features that can be created because of limitations of mechanical stability. In addition to cumbersome fabrication processes, the problem of slow flow rate and imperfect mixing leading to non-uniform colorimetric signals[5] remain the major challenges for multiplex colorimetric detection in µPADs.

In this article, we introduce a new device design called barrier-free microfluidic paper analytical device (BF-µPAD) that can simultaneously detect multiple targets without patterning barriers in paper. This was enabled by stacking two paper membranes with significantly different wicking rates. The top layer having a high wicking rate is used as a sample fluid

3

distributor, and detection reagents are spotted on the bottom membrane having a low wicking rate. The large difference in wicking rates ensures that the flow of sample fluid to the detection zones is predominantly in the vertical direction, from the top to the bottom membrane. Further, lateral flow in the bottom membrane is practically eliminated, obviating the need for barriers, and producing highly spatially uniform colorimetric signals. Our group has previously demonstrated the application of such an assembly in uniform rehydration of sample stabilization reagents stored on the bottom membrane, which aided in effective sample stabilization[6]. To better understand flow patterns in such an assembly, we present a Richards equation model of wicking flow in this stacked assembly. Richards equation[7] accounts for partial saturation in paper membranes and our group[8,9] and others[10,11] have previously established its use in modelling flow in paper microfluidic devices. We demonstrate the multiplexing feature of BF-μPAD by simultaneously testing four analytes thiocyanate[12], protein[3], glucose[4,13], and nitrite[14,15] in a 2cm x 2cm assembly. The barrier free assembly presented here overcomes important limitations of current single layer barrier-patterned μPADs.

EXPERIMENTAL SECTION

Materials and fabrication

Standard 17 glass fiber (referred to as 'Standard 17' here onward) and Whatman filter paper Grade 1 (referred to as 'filter paper' here onward) membranes were acquired from GE Healthcare Life Sciences (Bangalore, India). Transparent acrylic sheets of thickness 2.16 mm and 5 mm were acquired locally. All layered devices were fabricated using 2.16 mm acrylic sheets and circular fluid reservoirs were cut into 5 mm acrylic sheets. Double-sided pressure sensitive adhesive (PSA; 3M 9731) and PDMS tape (ARclad IS-7876) were used to secure the paper layers and acrylic sheets together. All designs were created in AutoCAD (Autodesk, San

Rafael, CA). All materials were cut using a 50 W CO_2 laser in a VLS 3.60 laser engraver (Universal Laser Systems, Scottsdale, AZ). Images were captured using a Redmi 5 smartphone and a Canon LiDE 220 flatbed scanner.

Chemicals and assays

All reagents and stock solutions were prepared in DI water unless otherwise mentioned. The pH experiment was performed using 10 mg/ml bromophenol blue solution (Sisco Research Laboratories Pvt. Ltd. India) as the dried reagent and 1 M HCl (Thomas Baker Chemicals Pvt. Ltd.) as the sample fluid. *Thiocyanate detection assay:* The assay for colorimetric detection of thiocyanate was adapted from Pena-Pereira et al.[12] Reagents for the test were prepared by dissolving 10.1g of $Fe(NO_3)_3.9H_2O$ in 20 ml of DI water followed by addition of 2 ml of 1 M nitric acid. The final volume was adjusted to 25 ml using DI water. Stock solution for thiocyanate detection was prepared as 1 M NaSCN. *Protein detection assay:* This assay was adapted from Martinez et al.[3] Detection reagents were prepared by mixing equal volumes of 250 mM citrate buffer (pH =1.8) and 3.3 mM bromophenol blue (Sisco Research Laboratories Pvt. Ltd. India) in 95% ethanol. Citrate buffer was prepared by dissolving10.5 mg of citric acid and 47.3 mg of sodium citrate in 10 ml of DI water. Bovine serum albumin (BSA; Sigma-Aldrich A2153), 20 mg/ml, was used as a stock solution for protein detection. *Glucose detection assay:* Glucose detection assay was adapted from Zhu et al.[4] and Santana-Jimenez et al.[13], and reagents were prepared by mixing equal volumes of glucose oxidase (20 mg/ml), horseradish peroxidase (1 mg/ml), 4-amino antipyrine (20 mg/ml), and 2,4,6-tribromo-3-hydroxybenzoic acid (5 mg/ml). Stock solution was prepared using dextrose (200 mg/dl). All chemicals for glucose testing were obtained from Sisco Research Laboratories Pvt. Ltd. India. *Nitrite detection assay:* Nitrite was detected by the Griess reaction as described by Klasner et al.[14] and Blicharz et al.[15] Equal volumes of 50 mM sulfanilamide (Sigma-Aldrich), 330 mM

citric acid, and 10 mM n-(1-napthyl) ethylenediamine in methanol were mixed. Stock solution for nitrite was prepared as a 100 mM solution of NaNO$_2$.

Reagents for thiocyanate, protein, and nitrite detection were stored at room temperature in amber centrifuge tubes and were used for 15 days without any noticeable loss of activity, while that for glucose detection were freshly prepared. Stock solution for thiocyanate and nitrite detection were stored at 4˚C and used for one week without recording loss of signal while that of glucose and BSA were freshly prepared. For paper-based assays, reagents were manually pipetted on the paper and dried for 15 min followed by device assembly and immediate introduction of sample. The following chemicals were obtained as kind gifts: sodium thiocyanate, ferric nitrate, methanol, sodium nitrite, citric acid, and sodium citrate from Dr Venugopal Santhanam, and n-(1-napthyl) ethylenediamine from Prof Santanu Bhattacharya (both from IISc, Bangalore).

Image analysis and determination of limits of detection

All images were analyzed in ImageJ software. Color images (8-bit) were first split into red, blue, and green channels. For the pH experiment and thiocyanate assay, signal intensities were measured using the blue channel; for glucose and nitrite assays using the green channel; and for protein assay using the red channel. A circular region of interest (ROI) covering ~80% of the diameter of the signal was created to measure the mean intensity, I, of a signal spot; the size of the ROI was fixed for all analyses. The blank signal, I_{blank}, measured as the mean (N=3) of the signal intensity generated by introducing DI water into identical detection zones was subtracted from all test signals. Prior to subtraction, all intensities were inverted by subtracting from 255 to account for generation of colored spots over a white background. Final signal intensities were thus reported as $I_{test} = (255 - I) - (255 - I_{blank})$. The limits of detection

for BF-μPAD and μPAD were calculated using a 4-parameter logistic curve described by Holstein et al[16]. The method includes variance of mean of all data points performed in replicates (N=4) for 7 different analyte concentrations including the blank.

MODELLING SECTION

To understand fluid flow profiles in BF-μPAD, the device was modelled in COMOSL Multiphysics 5.4 software using Richards equation using methods previously described by our group[8,9]. Liquid imbibition in porous media, considering partial saturation, is described by Richards equation as:

$$\frac{\partial \theta}{\partial t} = \nabla.\left(\frac{\kappa(\theta)}{\mu} \nabla(\psi(\theta) + \rho g z)\right) \text{--------(1)}$$

where θ is volumetric liquid content in the membrane, ψ is capillary pressure (Pa) induced by the membrane on the liquid, κ is permeability (m^2) of the membrane, and μ is viscosity (Pa.s) of the liquid. Since the assembly was kept horizontal and the membranes were very thin ($\sim 10^{-4}$ m), gravitational head $\rho g z$ was neglected. A normalized saturation parameter was defined as $Se = (\theta - \theta_r)/(\theta_s - \theta_r)$, where θ_s is the maximum volumetric content at saturation, θ_r is the residual volumetric content (assumed to be 0). θ varies from θ_r to θ_s and therefore Se varies from 0 to 1. In order to solve the Richards equation, ψ and κ as a function of Se must be known for each porous material. A popular set of constitutive relations for $\kappa(Se)$ and $\psi(Se)$ is the Van Genuchten formulation that involves three parameters: α, n, l for each material. These parameters were obtained by fitting experimental data for $\psi(Se)$ for Standard 17 and filter paper previously acquired in our lab[6]. Details of the Van Genuchten formulation and all parameters used for COMSOL simulations are provided in Supporting Information (SI) Section 1.

RESULTS AND DISCUSSION

Design and function of BF-µPAD

BF-µPAD consists of a stack of a Standard 17 membrane placed flush on top of a filter paper membrane (Fig. 1A). Reagents for analyte detection are spotted at distinct locations in the filter paper membrane and the sample fluid is added on top of the Standard 17 membrane (Fig. 1A). The top Standard 17 layer has a higher wicking rate compared to the bottom filter paper layer. The T_{4-cm}, i.e. time required for fluid to wick 4 cm from the source in horizontally placed membrane strips, are 12 s and 110 s for Standard 17 and filter paper, respectively[6].

Prior to multiplex detection, an 8 cm x 2 cm BF-µPAD was tested for uniformity of signals over the surface by depositing multiple spots of a pH dye on the detection layer (Fig. 1A). Sixteen 1 µl spots of 10 mg/ml bromophenol blue were hand pipetted on the detection layer using a custom-made 8 cm x 2 cm acrylic stencil containing equispaced holes of 0.6 mm radius. The generated spots were allowed to dry for 15 minutes at room temperature before placing the Standard 17 distribution layer on top. PSA layers, 8 cm x 2 cm, were used to adhere the detection layer to the bottom acrylic base and to adhere the distribution layer to the top acrylic cover. The top acrylic cover and the top PSA layer had 4 mm radius holes at the center for sample introduction. The entire assembly was secured with PDMS tape along the longer edges to prevent fluid leakage. A fluid reservoir made out of acrylic was adhered on the top acrylic cover. The top and bottom acrylic layers had small protrusions on both ends (Fig. 1A) to enable supporting the device at an elevation to enable imaging from both sides.

A direct comparison of colorimetric signal development in BF-µPADs and control devices was performed. A control device consisted of a single 8 cm x 2 cm filter paper detection layer spotted identically with reagents but lacking the top distributor layer (Fig. 1B). For this, a 1 M

HCl solution was introduced into both: 255 µl in control and 895 µl in BF-µPAD. These volumes were chosen to match the fluid absorption capacities of the respective devices. On addition of acid, the blue pH indicator changes color to yellow. When HCl was added to control, by the time the fluid fully wet the membrane (t = 150s), the yellow spots merged into each other generating smudges of yellow color (Fig. 1B; Control). However, the BF-µPAD generated 16 distinct signal spots (Fig. 1B; BF-µPAD), even though the detection regions were not separated by physical barriers. Further, the time of rehydration reduced to 30s owing to the rapid wicking rate of the distribution layer. The smudges in control are explained by the laterally wicking fluid pushing (convecting) the dried reagents along with it. On the other hand, in BF-µPAD, the lateral flow primarily occurs in the distribution layer; there is practically zero lateral flow in the bottom detection layer. These flow patterns are modelled in the following section.

The uniformity of signal across all 16 spots in the BF-µPAD was then assessed. Fig. 1C shows the mean intensity of the 16 spots when imaged from the bottom (detection layer side) using a flatbed scanner (empty squares; Fig. 1C) and a smartphone camera (solid circles; Fig. 1C). Error bars represent standard deviations in mean intensities at each spot location across three replicates of the device. There was no statistically significant difference in the mean intensity across the 16 spots, which confirms that the performance of a detection spot is not dependent on its distance from the fluid source. Coefficients of variation in mean intensity of all 48 spots across 3 replicate devices were 6.94% when imaged by a smartphone and 3.49% when imaged using a flatbed scanner. While demonstrated using 16 detection spots here, an 8 cm x 2 cm BF-µPAD can also incorporate 20 reagent spots of 1 µl each of pH dye (SI Section S2 and Movie S1) and 32 reagent spots of 0.4 µl each of glucose assay (SI section S2 and Movie S2).
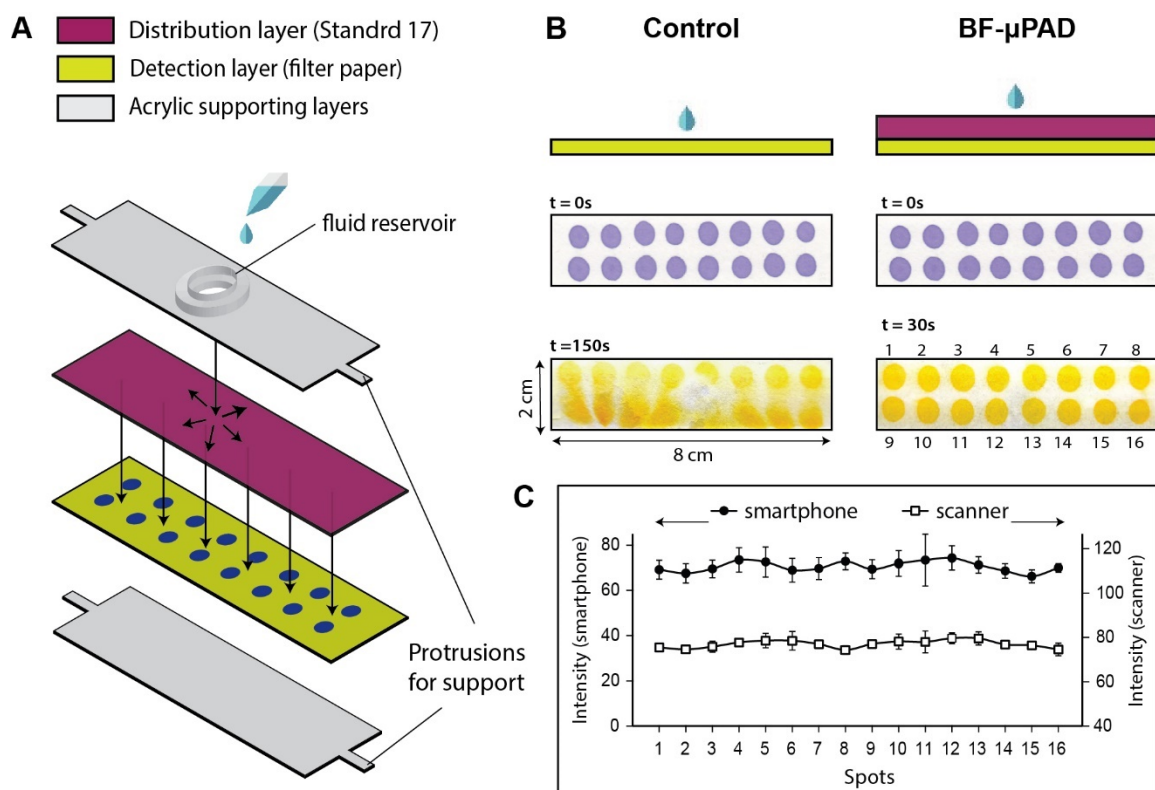
9

Figure 1. Design and function of BF-µPAD. **(A)** Schematic of an 8 cm x 2 cm device containing 16 detection zones. Sample added through the reservoir flows rapidly through the Standard 17 distribution layer and acts as a source for rehydrating the detection reagents in the filter paper detection layer directly underneath. **(B)** Comparison of rehydrated reagents with and without the distribution layer, on addition of 1M HCl. In control, rehydrated reagents merge into each other, while in BF-µPAD, all 16 rehydrated reagent spots remain segregated. **(C)** End-point color intensities of the 16 detection spots in BF-µPAD for images captured by a smartphone and a flatbed scanner. Error bars represent standard deviations (N=3).

Modelling flow in an assembly of Standard 17 and filter paper

Wicking flow in an assembly of a Standard 17 layer placed on top of a filter paper membrane was modelled using Richards equation to understand flow patterns. Our group has previously demonstrated the use of Richards equation in modeling wicking flow through a serial assembly of two different membranes[9]. However, this is the first demonstration of the use of Richards equation for modelling flow through a stack of paper membranes. For this, a 2D spatial domain is considered – x direction being the direction of lateral flow along the length of the device,

and y direction being the vertical direction spanning the thickness of the two membranes (Fig. 2A). Because the flow profile would be uniform around the central fluid reservoir, only half of the device was modelled, representing a side view of the assembly (Fig. 2A). The top rectangle (or domain) represents the 370 μm thick Standard 17 distribution layer and the bottom rectangle represents the 180 μm thick filter paper detection layer (Fig. 2A). Fluid inlet was represented by a 4 mm horizontal line at $y = 0$, initiating from the origin. Note that the representation of the domain in Fig. 2A is not to scale.

The Richards equation solves for Se, the normalized saturation, as a function of space and time. Therefore, boundary conditions and initial conditions are needed on Se, which is directly correlated to capillary pressure, ψ, for each material (SI Section S1).

Boundary conditions: Fluid reservoir was assumed to be fully saturated, so an inlet condition, $Se = 1$, was imposed along the 4 mm horizontal fluid entry line at $y = 0$. A symmetric boundary condition was imposed along the y axis. A flux continuity boundary condition was assigned to the common edge of the two rectangles. All other edges in the model geometry were set to a non-flux Neumann boundary condition.

Initial condition: Initially, both membranes were dry, i.e. $Se = 0$. However, ψ asymptotically reaches infinity at $Se = 0$, which causes computational errors. Therefore, Se corresponding to the maximum experimentally measured capillary pressure at which the model produced wicking rates that matched experimental observations were set as the initial conditions for both domains (see SI Section S1).

Convective velocity in partially saturated domains is given by[9]:

$$velocity = \frac{\kappa(\theta)}{\mu} \nabla\big(\psi(\theta)\big) \text{-----------(2)}$$

After solving the model, horizontal (u) and vertical (v) velocity components in the two domains were extracted using 6 spatial points – 1 cm, 2 cm, and 3 cm from the origin in the x direction, and at the centers of the two domains in the y direction (-185 μm and -460 μm for top and bottom domain, respectively; Fig. 2A). In the top domain, horizontal velocity, u, decreased over time for all three spatial points (Washburn-like behavior), ultimately reaching zero at full membrane saturation (Fig. 2B(i)). On the other hand, the vertical velocity, v, at all three points in the top domain was ephemeral and appeared as sharp spikes at time points when the fluid fronts reached those spatial points (Fig. 2B(ii)). Moreover, the magnitudes of v are ~1 order of magnitude lower than that of u (Fig. 2B (i)-(ii)). These spikes in vertical velocity, v, represent movement of the fluid from the top to the bottom domain. The short durations of these spikes suggest that the membranes saturate rapidly in vertical direction. A similar analysis was conducted for the chosen spatial points in the bottom membrane. In stark contrast to the top domain, the horizontal velocity, u, in the bottom domain only appeared as spikes (Fig. 2B(iii)). Vertical velocities, v, in the bottom domain reflect those in the top domain and also appear as spikes (Fig. 2B(iv)) with peak velocities being ~1 order of magnitude less than horizontal velocities, u. Two important observations may be made from these data: a) the dominant direction of flow in the assembly is the horizontal direction, and b) there is no continuous flow of fluid in any direction in the bottom membrane. These observations were corroborated by a direct comparison of horizontal velocities, u, in the top and bottom domains along horizontal lines ($x = 0$ to 4 cm) at $y = -185$ μm (top domain) and $y = -460$ μm (bottom domain) (Fig. 2C). Velocities were extracted at three different time points – 5s, 10s, and 15s. In the top domain, non-zero velocities exist all the way up to the fluid fronts (solid lines; left y-axis; Fig. 2C), while in the bottom domain, non-zero velocities exist only locally in the vicinity of the fluid fronts (dotted lines; right y-axis; Fig. 2C). Further, the magnitude of horizontal velocity is about an order of magnitude higher in the top domain compared to bottom (left vs right y-axis; Fig.
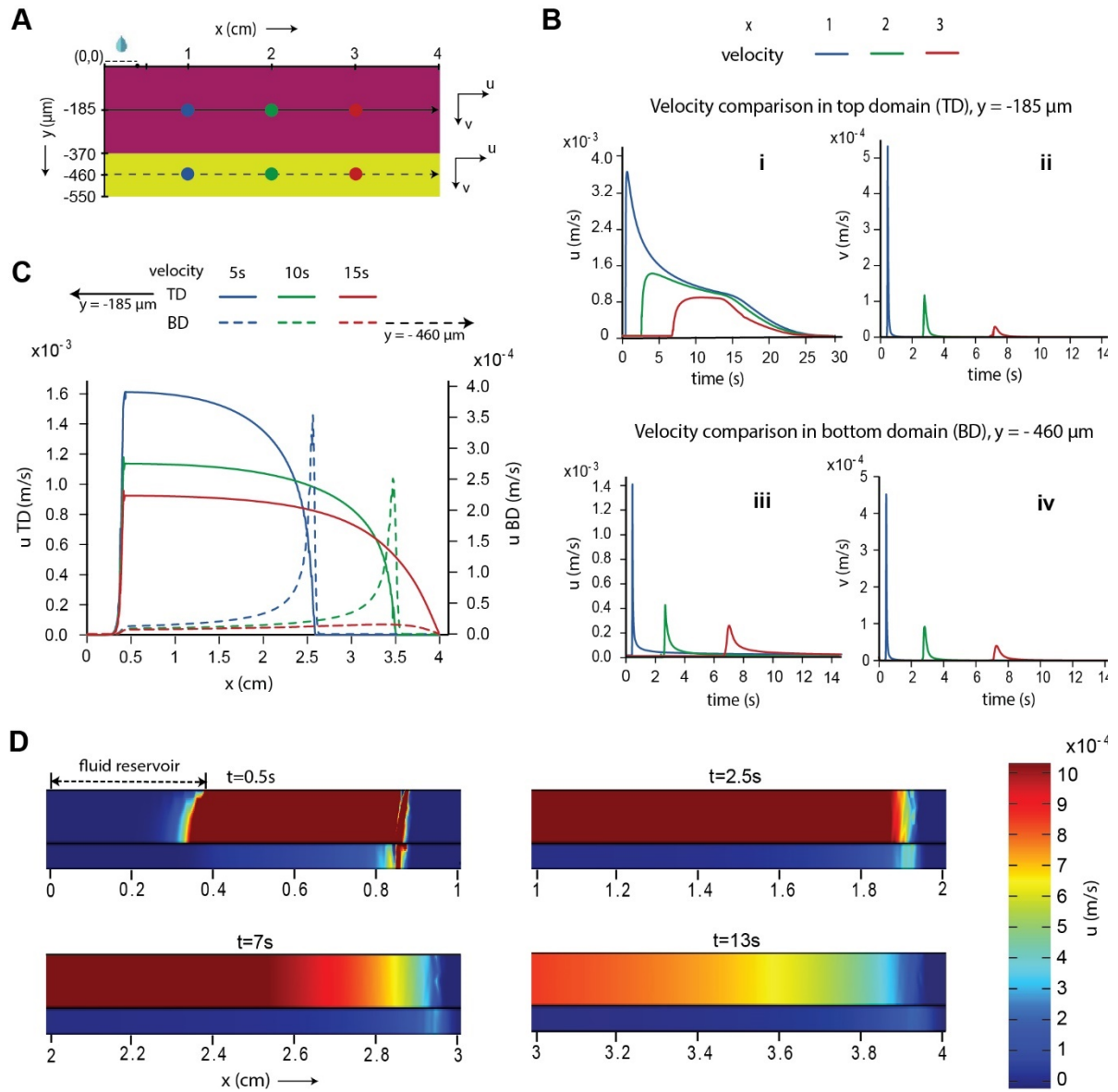
Figure 2. Results of flow modelling. **(A)** Model geometry representing side view of BF-µPAD with a 4 mm horizontal line at $y=0$ as the fluid inlet. **(B)** Comparison of horizontal (u) and vertical (v) velocity components at three different x locations along the centers of membrane thicknesses for top domain **(i, ii)** and bottom domain **(iii, iv)**. **(C)** Variation of lateral flow velocity along 4 cm horizontal lines passing through the centers of membrane thicknesses at three different time points. **(D)** Surface plots of horizontal velocity profiles at different time points.

2C). Surface plots of horizontal velocity, u, at different time points ($t = 0.5$s, 2.5s, 7s, and 13s)

shed more light on the flow patterns (Fig. 2D). While the top domain contains large regions

having a significant convective velocity at any time, the bottom domain only has local regions

of convection just below where the fluid fronts exist in the top domain. Further, these local convective velocities are temporary (Fig. 2B(iii)-(iv)).

From these results, the following can be concluded about wicking flow in the BF-μPAD assembly. Fluid introduced into the top layer wicks rapidly away from the source in the lateral direction and continuously feeds fluid to the bottom layer in the vertical direction. As soon as the bottom layer receives fluid, it saturates and there is no more movement of fluid in the bottom layer. Instead, the unsaturated regions of the bottom membrane continue to receive fluid from the top distribution layer. This explains why rehydrated reagents in the detection layer of BF-μPAD do not move away from their locations via convection, enabling barrier-free multiplex detection. Note that diffusion of rehydrated reagents would still occur in the bottom domain and could carry reagents away from the detection zones, but the time scale for diffusion is significantly longer than the test time; within the time span of the detection experiment (< 6 min), diffusion over these length scales may be safely neglected.

Multiplex detection in BF-μPAD

The application of BF-μPAD for multiplex colorimetric detection is demonstrated next using a 2 cm x 2 cm device containing 4 analyte detection zones, prepared by manually pipetting 1 μl each of the corresponding colorimetric detection reagent. The user experience is shown in Fig. 3A; the user is required to add a predefined sample volume equal to volumetric capacity of the two membranes into the sample reservoir (244 μl for a 2 cm x 2 cm device), wait for 30 seconds for the sample to saturate the assembly and develop signal, and flip the device to image the bottom layer using a smartphone. Multiplexing is demonstrated using four clinically relevant analytes: thiocyanate (SCN^-), protein (BSA), glucose, and nitrite (NO_2^-)[3,4,12–15]. While all these analytes are adequately present in saliva, the demonstration here uses samples

14

prepared in DI water. However, our group has previously demonstrated that such a stacked assembly is compatible with flow of more viscous fluids like sputum[6]. Eight different samples having varying concentrations of the 4 analytes were prepared. Concentrations were chosen such that they spanned the clinically relevant range of these analytes in saliva. Fig. 3B shows an actual fabricated BF-μPAD device before sample addition, along with the locations of the four detection reagents. The SCN^- reagent turns colorless to brown, glucose and NO_2^- reagents turn colorless to pink, and the BSA reagent changes from yellow to blue with increasing analyte concentration. Results of detection from 8 different samples containing SCN^- ion and glucose concentrations in decreasing order and BSA and NO_2^- ion concentration in increasing order (from top to bottom row) are shown in Fig. 3C. Four distinct reaction zones were maintained throughout the test. The intensity of color generated over the circular ROI for each analyte increased monotonously with increasing analyte concentration (Fig. 3D).
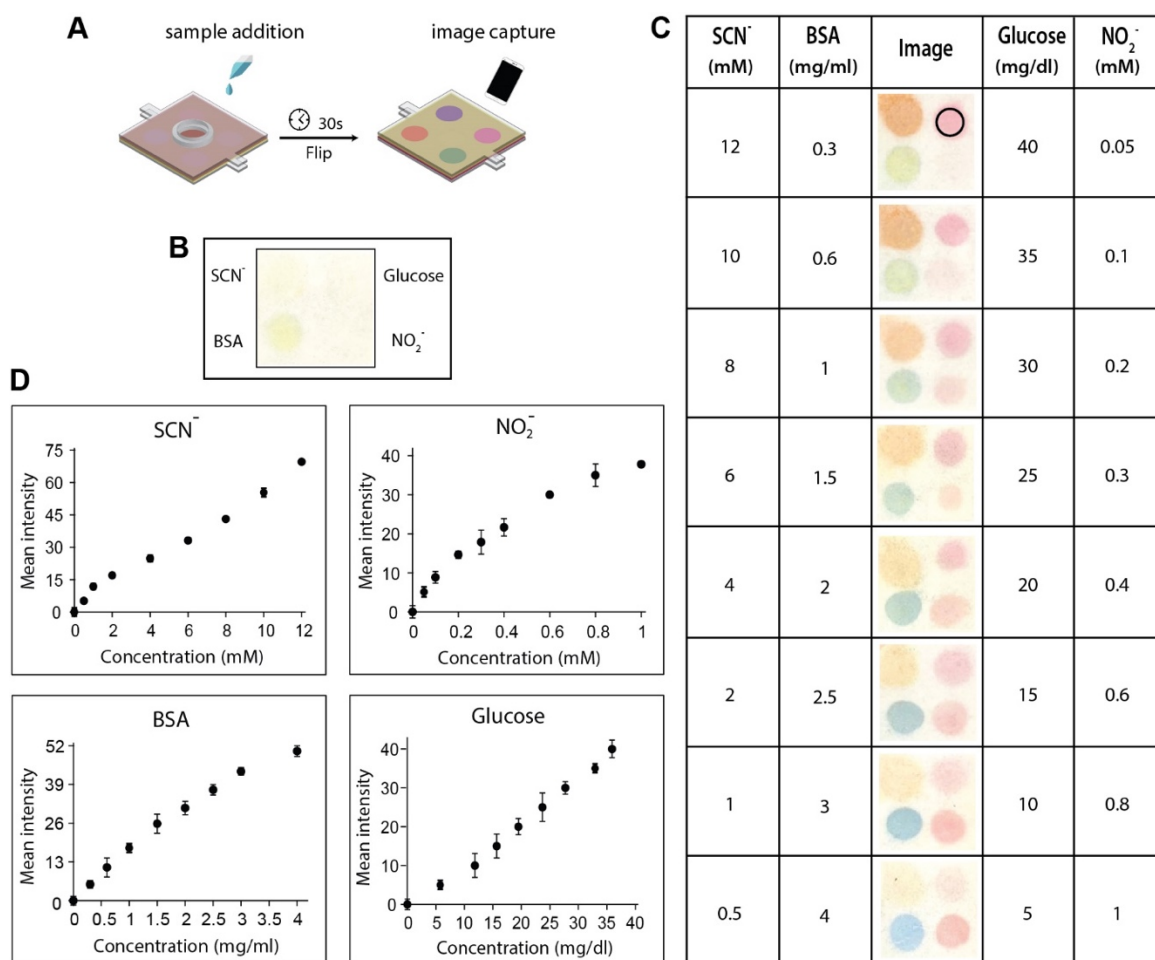

SCN^- (mM)	BSA (mg/ml)	Image	Glucose (mg/dl)	NO_2^- (mM)
12	0.3		40	0.05
10	0.6		35	0.1
8	1		30	0.2
6	1.5		25	0.3
4	2		20	0.4
2	2.5		15	0.6
1	3		10	0.8
0.5	4		5	1

Figure 3. Multiplex detection in BF-µPAD. **(A)** The user experience: the user adds the sample into the reservoir, waits for 30s, flips the device and captures the result using a smartphone. **(B)** Image of filter paper-side of BF-µPAD with dried reagents before sample addition. **(C)** Results from BF-µPAD after introduction of samples containing different concentrations of 4 analytes: thiocyanate, BSA, glucose, and nitrite. Black circle around 40 mg/dl glucose shows the representative region of interest for signal analysis. **(D)** Calibration plots for thiocyanate, nitrite, BSA, and glucose. Error bars represent standard deviations (N=3).

Investigation on cross-mixing

Because BF-µPADs lack flow barriers in between detection zones, it was important to determine whether reagents from one detection zone affected colorimetric signals in another detection zone directly downstream the convective flow. For this, two types of 4 cm x 2 cm BF-µPADs were fabricated – a singleplex device with 4 nitrite detection spots at four corners (Fig. 4A; singleplex device) and a multiplex device containing 2 spots each for glucose and BSA detection, in addition to the 4 nitrite detection spots (Fig. 4A; multiplex device). In the multiplex device, the nitrite-containing sample introduced into the sample reservoir must flow over the region containing detection zones for BSA and glucose. Solutions containing 4 different nitrite ion concentrations and one blank solution were added as a sample fluid to both devices. The signal intensity of nitrite detection zones increased monotonously with increasing nitrite ion concentration and the signal response was identical for the singleplex and multiplex devie (Fig. 4B). Students t-test comparison of signal intensities for singleplex vs multiplex devices at all nitrite concentration produced P values > 0.41 (N=4), showing that the signals were virtually indistinguishable. It may be noted that the developed pink color for different nitrite concentrations in this experiment was visibly darker than the corresponding pink color produced in the previous multiplex detection experiment (Fig. 3C). This is because the nitrite assay develops signal slowly and, in this analysis, we waited for the color to fully develop and captured images after 6 minutes of sample addition. The longer wait time ensured that enough time was provided for cross reactivity between reagent zones to occur, if any. However, no

16

cross reactivity was found. In a separate set of experiments, the specificity of the colorimetric assays within paper were tested to check whether the presence of multiple analytes in the sample affected the performance of any particular colorimetric assay (SI Section 3). No such cross reactivity was found.
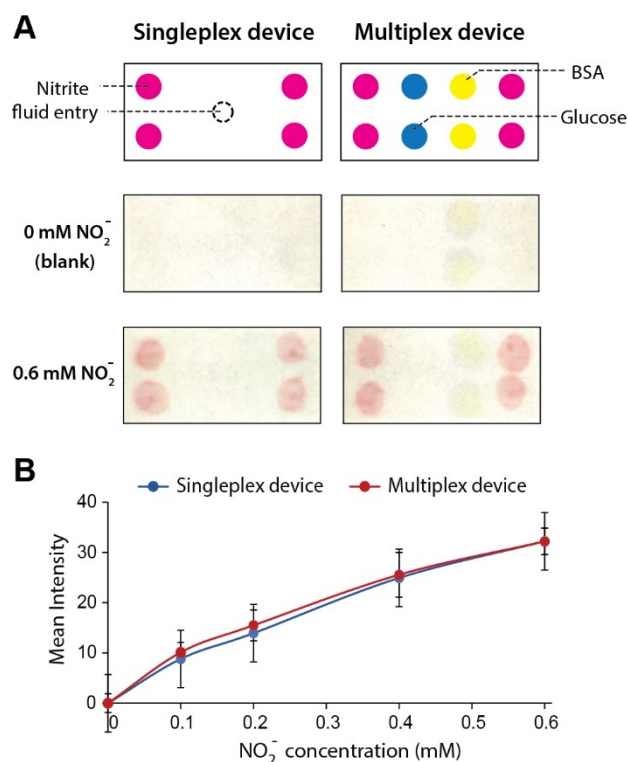

Figure 4. Investigations of reagent cross mixing in BF-μPAD. **(A)** Test results from a singleplex BF-μPAD containing detection spots for nitrite, and from a multiplex BF-μPAD containing detection spots for BSA and glucose in addition to nitrite. Top row: schematic; middle and bottom rows: results from blank and 0.6 mM NO_2^- solution, respectively. **(B)** Variation of mean intensity with NO_2^- concentration in singleplex and multiplex devices. Error bars represent standard deviations (N=4).

Comparative performance of BF-μPAD and μPAD

The performance of the colorimetric assay for the detection of BSA in a 4-zone BF-μPAD (Fig. 5A; top row) was compared to that in a conventional single layer μPAD made from filter paper (Fig. 5B; bottom row). The single layer μPADs tested here did not contain wax or hydrophobic barriers; instead flow channels were created by cutting the desired paper shapes using a laser cutter (Fig. 5B; bottom row). These devices replicate the flow patterns and rehydration profiles

17

found in conventional wax patterned single layer μPADs. Dimensions of the laser cut μPADs are provided in SI section 4. Sample solutions containing six different BSA concentrations were introduced into the two types of devices – μPADs and BF-μPADs. Sample volumes were 22 μl and 244 μl for μPADs and BF-μPADs, respectively, chosen to match the volumetric capacities of the two devices. Images were acquired using a smartphone camera, 6 minutes after sample introduction. When 0.1 mg/ml and 0.2 mg/ml BSA were added to μPAD, the signals were undistinguishable from blank (0 mg/ml BSA; Fig. 5A; bottom row), whereas when these samples were added in BF-μPAD, faint but distinguishable blue color was generated (Fig. 5A; top row). Further, at all concentrations, blue color in single layer μPADs only developed near the inlet to the detection zone, producing non-homogeneous signals over the circular detection zones (Fig. 5A; bottom row). On the contrary, homogeneous colorimetric signals were generated at all concentrations in BF-μPAD (Fig. 5A; top row). Uniformity in signals in BF-μPAD is a result of rehydration of the reagents in the vertical direction from the distribution layer and a near absence of convection in the bottom detection layer.

A direct comparison of the limits of detection (LODs) for the two devices was then performed using the method described by Holstein et al[17] (insert ref again). Detailed calculations of LOD are provided in supporting information (SI section 4). For the BSA assay performed in BF-μPAD, the LOD and corresponding 95% confidence interval (CI) were found to be 0.1817 and 0.1283-0.3682 mg/ml, respectively calculated. For the same assay performed in μPAD, the LOD and corresponding 95% confidence interval were found to be 0.6727 and 0.5314-0.8217, respectively. BF-μPADs thus improved the LOD by 3.7x compared to single layer μPADs. Fig. 5B shows the variation of signal intensity with BSA concentration, and LOD and 95% CI for BF-μPAD and μPAD. This improvement in LOD is at least in part because of the ability of BF-μPAD to probe a larger volume of sample residing in the combination of the two layers. At

low analyte concentration, analyte molecules are limiting while the detection reagent molecules are in excess. By enabling the detection reagents to interact with a greater number of analyte molecules in the combination of two layers in BF-µPAD, more product is formed and therefore the LOD improves. This advantage may be lost at higher analyte concentrations where the analyte may no longer be limiting (Fig. 5B; 2 mg/ml BSA).
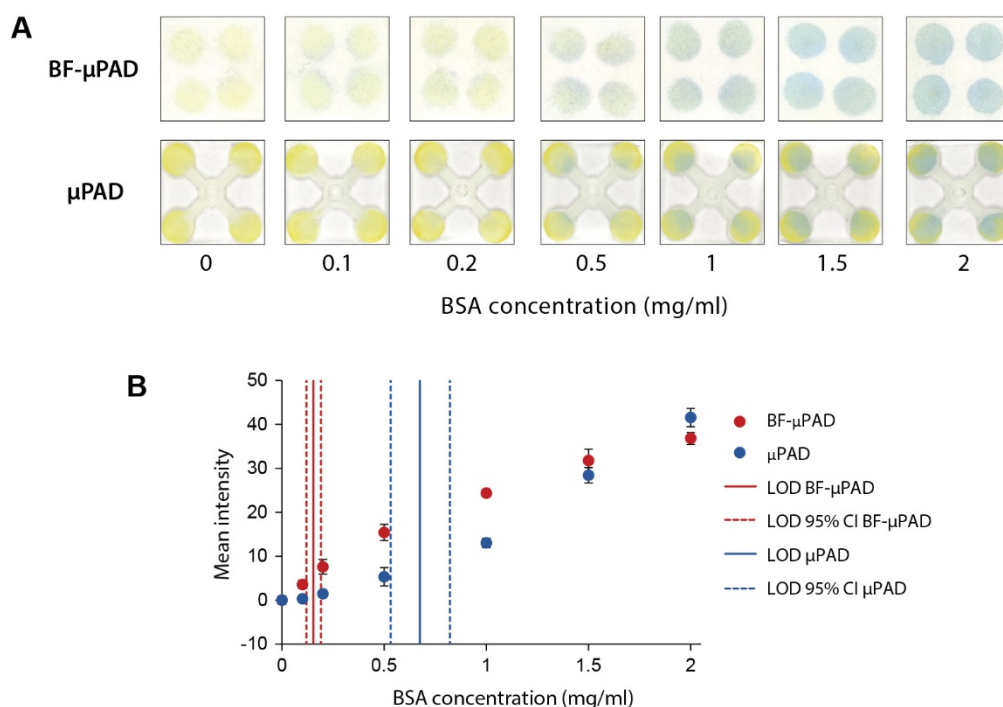

Figure 5. Comparison of LOD between BF-µPAD and µPAD. **(A)** End point image of detection layer of BF-µPAD and µPAD at different BSA concentration. **(B)** Variation of blue colored intensity in BF-µPAD and µPAD with BSA concentration. LOD and its 95% confidence interval reveal that BF-µPAD has better sensitivity than µPAD. (N=4)

Overall, we have demonstrated a new paper-based device design that enables multiplex colorimetric detection from fluid samples without pattering paper with physical barriers. The new BF-µPAD design improves the LOD compared to conventional µPADs. However, compared to conventional µPADs, BF-µPADs require larger sample volumes, which may be a shortcoming. But for several sample types like saliva, urine, environmental wastewater, food and beverages etc. larger sample volumes are readily available. BF-µPAD is based on a

strategic combination of two porous membranes that produce a desired flow pattern. While different combinations of paper materials[6,18] and combinations of papers with ducts[19,20] have been developed for manipulating flow rates in paper channels, their utilization for multiplex colorimetric detection is first demonstrated in this article. An important advantage of BF-μPAD over conventional μPADs is that it would be more compatible with viscous fluids and emulsions like milk etc., which are difficult to flow through cellulosic membranes alone. The Standard 17 layer in BF-μPADs has a significantly larger permeability and enables the flow of viscous fluids as our group has previously demonstrated using sputum samples[6]. This work also advances the area of modelling wicking flow in paper membranes – this is the first report of the use of Richards equation to model flow in a stack of paper membranes having different wicking properties.

In this work, reagents were manually deposited using a plastic stencil to guide the pipette to desired locations, which led to inconsistent shape and size of reaction zone. This issue can easily be overcome using automated reagent dispensers, which are any way needed for the large-scale fabrication of conventional μPADs. Out of the 4 colorimetric assays, three assays generated self-contained circular colorimetric signals, but the thiocyanate assay produced signals that spread outside the detection zone (Fig. 3C). This is likely because the thiocyanate assay generates color instantaneously and some colored product diffuses back into the top layer where it moves away from the source by convection. The other three colorimetric reactions were slower and took of the order of 2-5 minutes for the color to fully develop, by which time, there was no more convection in the top layer. This puts a theoretical limit on the types of assays that can be incorporated in BF-μPAD for generation of self-contained signals – the rate of reaction must be slower than the rate of convection in the distribution layer. However, if this

is not possible, assays that generate color instantaneously must be placed at the corners of the device, so the colored product does not convect into downstream reaction zones.

CONCLUSION

The BF-µPAD design overcomes two important limitations of existing µPADs while improving upon the LODs – i) the need to pattern paper with physical barriers like wax, and ii) spatially non-uniform colorimetric signal generation. Obviating the need to pattern physical barriers will significantly reduce the infrastructure associated with manufacturing of paper-based analytical devices. The only instrument needed to manufacture BF-µPADs at a large scale would be a benchtop reagent dispensing robot that can handle microliter volumes, which are widely available commercially. Our future work on the development of BF-µPAD would include systematically studying combinations of distributor and detection layer materials for optimized performance, testing compatibility with viscous samples, and deployment of BF-µPADs for field testing.

ASSOCIATED CONTENT

Supporting Information. The following Supplementary Information is available free of charge on the ACS Publications website.

S1: COMSOL modelling details; S2: uniform rehydration of 20 spots on a BF-µPAD; S3: Effect of interfering species on signal intensity; S4: Comparison of signal intensity in BF-µPAD and µPAD. (PDF document).

Rehydration of 20 detection spots (Movie S1)

Rehydration of 32 detection spots (Movie S2)

AUTHOR INFORMATION

Corresponding author

*E-mail: bhushan@iisc.ac.in. Phone: +91-80-2293-3114.

Author Contributions

B.J.T contributed towards conception and design of the work, obtaining funding, and analysis and interpretation of data. A.C conducted all experiments and contributed towards design of the work and analysis and interpretation of data. B.J.T and A.C together wrote the main manuscript text and prepared figures.

Notes

The authors declare no competing financial interest.

REFERENCES:

(1)   Yang, Y.; Noviana, E.; Nguyen, M. P.; Geiss, B. J.; Dandy, D. S.; Henry, C. S. Paper-Based Microfluidic Devices: Emerging Themes and Applications. *Anal. Chem.* **2017**, *89* (1), 71–91. https://doi.org/10.1021/acs.analchem.6b04581.

(2)   Cate, D. M.; Adkins, J. A.; Mettakoonpitak, J.; Henry, C. S. Recent Developments in Paper-Based Microfluidic Devices. *Anal. Chem.* **2015**, *87* (1), 19–41. https://doi.org/10.1021/ac503968p.

(3)   Martinez, A. W.; Phillips, S. T.; Butte, M. J.; Whitesides, G. M. Patterned Paper as a Platform for Inexpensive, Low-Volume, Portable Bioassays. *Angew. Chemie - Int. Ed.* **2007**, *46* (8), 1318–1320. https://doi.org/10.1002/anie.200603817.

(4)   Zhu, W. J.; Feng, D. Q.; Chen, M.; Chen, Z. D.; Zhu, R.; Fang, H. L.; Wang, W. Bienzyme Colorimetric Detection of Glucose with Self-Calibration Based on Tree-Shaped Paper Strip. *Sensors Actuators, B Chem.* **2014**, *190*, 414–418. https://doi.org/10.1016/j.snb.2013.09.007.

(5)   Evans, E.; Moreira Gabriel, E. F.; Benavidez, T. E.; Tomazelli Coltro, W. K.; Garcia, C. D. Modification of Microfluidic Paper-Based Devices with Silica Nanoparticles. *Analyst* **2014**, *139* (21), 5560–5567. https://doi.org/10.1039/c4an01147c.

(6)   Das, D.; Dsouza, A.; Kaur, N.; Soni, S.; Toley, B. J. Paper Stacks for Uniform Rehydration of Dried Reagents in Paper Microfluidic Devices. *Sci. Rep.* **2019**, *9* (1), 1–12. https://doi.org/10.1038/s41598-019-52202-9.

(7)   Richards, L. A. Capillary Conduction of Liquids through Porous Mediums. *J. Appl. Phys.* **1931**, *1* (5), 318–333. https://doi.org/10.1063/1.1745010.

(8)   Rath, D.; Sathishkumar, N.; Toley, B. J. Experimental Measurement of Parameters Governing Flow Rates and Partial Saturation in Paper-Based Microfluidic Devices. *Langmuir* **2018**, *34* (30), 8758–8766. https://doi.org/10.1021/acs.langmuir.8b01345.

(9)   Rath, D.; Toley, B. J. Modeling-Guided Design of Paper Microfluidic Networks: A Case Study of Sequential Fluid Delivery. *ACS Sensors* **2021**. https://doi.org/10.1021/acssensors.0c01840.

(10)   Jaganathan, S.; Tafreshi, H. V.; Pourdeyhimi, B. A Realistic Modeling of Fluid

Infiltration in Thin Fibrous Sheets. *J. Appl. Phys.* **2009**, *105* (11). https://doi.org/10.1063/1.3141737.

(11)   Perez-Cruz, A.; Stiharu, I.; Dominguez-Gonzalez, A. Two-Dimensional Model of Imbibition into Paper-Based Networks Using Richards' Equation. *Microfluid. Nanofluidics* **2017**, *21* (5), 1–12. https://doi.org/10.1007/s10404-017-1937-0.

(12)   Pena-Pereira, F.; Lavilla, I.; Bendicho, C. Paper-Based Analytical Device for Instrumental-Free Detection of Thiocyanate in Saliva as a Biomarker of Tobacco Smoke Exposure. *Talanta* **2016**, *147*, 390–396. https://doi.org/10.1016/j.talanta.2015.10.013.

(13)   Santana-Jiménez, L. A.; Márquez-Lucero, A.; Osuna, V.; Estrada-Moreno, I.; Dominguez, R. B. Naked-Eye Detection of Glucose in Saliva with Bienzymatic Paper-Based Sensor. *Sensors (Switzerland)* **2018**, *18* (4), 1–12. https://doi.org/10.3390/s18041071.

(14)   Klasner, S. A.; Price, A. K.; Hoeman, K. W.; Wilson, R. S.; Bell, K. J.; Culbertson, C. T. Paper-Based Microfluidic Devices for Analysis of Clinically Relevant Analytes Present in Urine and Saliva. *Anal. Bioanal. Chem.* **2010**, *397* (5), 1821–1829. https://doi.org/10.1007/s00216-010-3718-4.

(15)   Blicharz, T. M.; Rissin, D. M.; Bowden, M.; Hayman, R. B.; DiCesare, C.; Bhatia, J. S.; Grand-Pierre, N.; Siqueira, W. L.; Helmerhorst, E. J.; Loscalzo, J.; Oppenheim, F. G.; Walt, D. R. Use of Colorimetric Test Strips for Monitoring the Effect of Hemodialysis on Salivary Nitrite and Uric Acid in Patients with End-Stage Renal Disease: A Proof of Principle. *Clin. Chem.* **2008**, *54* (9), 1473–1480. https://doi.org/10.1373/clinchem.2008.105320.

(16)   Holstein, C. A.; Griffin, M.; Hong, J.; Sampson, P. D. Statistical Method for Determining and Comparing Limits of Detection of Bioassays. *Anal. Chem.* **2015**, *87*

(19), 9795–9801. https://doi.org/10.1021/acs.analchem.5b02082.

(17)   Holstein, C. A.; Griffin, M.; Hong, J.; Sampson, P. D. Statistical Method for

Determining and Comparing Limits of Detection of Bioassays. *Anal. Chem.* **2015**, *87*

(19), 9795–9801. https://doi.org/10.1021/acs.analchem.5b02082.

(18)   Toley, B. J.; Mckenzie, B.; Liang, T.; Buser, J. R.; Yager, P.; Fu, E. Tunable-Delay

Shunts for Paper Micro Fl Uidic Devices. **2013**.

(19)   Channon, R. B.; Nguyen, M.; Scorzelli, A.; Henry, E.; Volckens, J.; Dandy, D.; Henry,

C. Rapid Flow in Multilayer Microfluidic Paper-Based Analytical Devices. *Lab Chip*

2018, *18* (1), 793–802. https://doi.org/10.1039/C7LC01300K.

(20)   Channon, R. B.; Nguyen, M. P.; Henry, C. S.; Dandy, D. S. Multilayered Microfluidic

Paper-Based Devices: Characterization, Modeling, and Perspectives. *Anal. Chem.*

2019, *91* (14), 8966–8972. https://doi.org/10.1021/acs.analchem.9b01112.

Barrier-free microfluidic paper analytical devices for multiplex colorimetric detection of analytes

Ayushi Chauhan, Bhushan J. Toley*

Department of Chemical Engineering
Indian Institute of Science
Bangalore, India

*Correspondence to:
Bhushan J. Toley
Department of Chemical Engineering
Indian Institute of Science Bangalore
Malleswaram
Bangalore 560012
Phone: +91-9146142296
Email: bhushan@iisc.ac.in

Table of Contents

Supporting Information
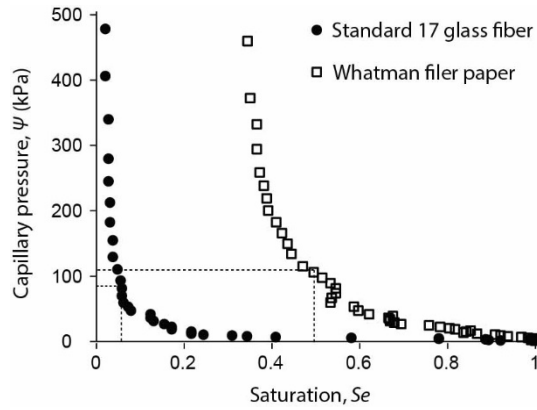
SI section 1. COMSOL modelling data

Figure S1. Capillary pressure vs saturation data for standard 17 glass fiber membrane (distribution layer) and Whatman filter paper grade 1 membrane (detection layer). Horizontal dashed lines represent the value of initial capillary pressure (P_o) of each membrane used in model.

Van Genuchten formulations:

We have used Van Genuchten equations to describe capillary pressure (ψ) and permeability (κ) as function of saturation (Se)[1]:

$$Se = \left(1 + \left(\frac{\alpha\psi}{\rho g}\right)^n\right)^{-m}$$

$$\kappa_r = Se^l\left(1 - \left(1 - Se^{1/m}\right)^m\right)^2$$

where $m = 1 - \frac{1}{n}$ and $\kappa_r = \frac{\kappa}{\kappa_s}$, $where$ κ_r is relative hydraulic conductivity, κ_s is saturated hydraulic conductivity and (α, n, l) are Van Genuchten parameters. Saturated permeability and saturated liquid content values were obtained from literature[1,2].

Parameters	Standard 17 glass fiber	Whatman filter paper
θ_s	0.9	0.7
$ks\,(m^2)$	5.63×10^{-11}	5.63×10^{-13}
$a\,(m^{-1})$	2.24	0.728
n	2.28	1.34
l	0.5	0.5
$P_o\,(kPa)$	-85	-110

Table S1. Characteristics of membrane used in COMSOL simulation

SI section 2. Study of uniform rehydration over larger number of spots

8cm x 2cm assembly of BF-µPAD was tested for 20 spots of 1 µl each of bromophenol blue dye. Device was assembled as described in main text (refer to "Design and function of BF-µPAD" section in main article). On addition of 1 M HCl, blue spots change to yellow and uniform rehydration was achieved for 20 spots device with statistically similar intensities for image taken by smartphone and flatbed scanner (Fig S2). This shows that the device can detect as much as 20 different chemistries independent of their distance from fluid entry source.
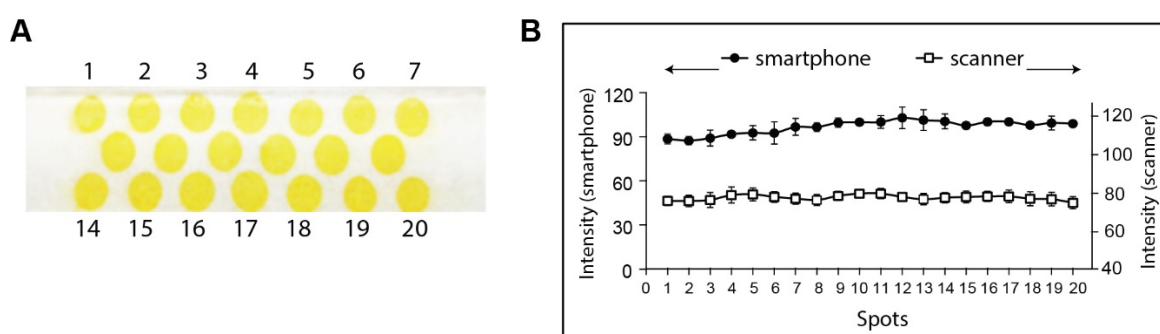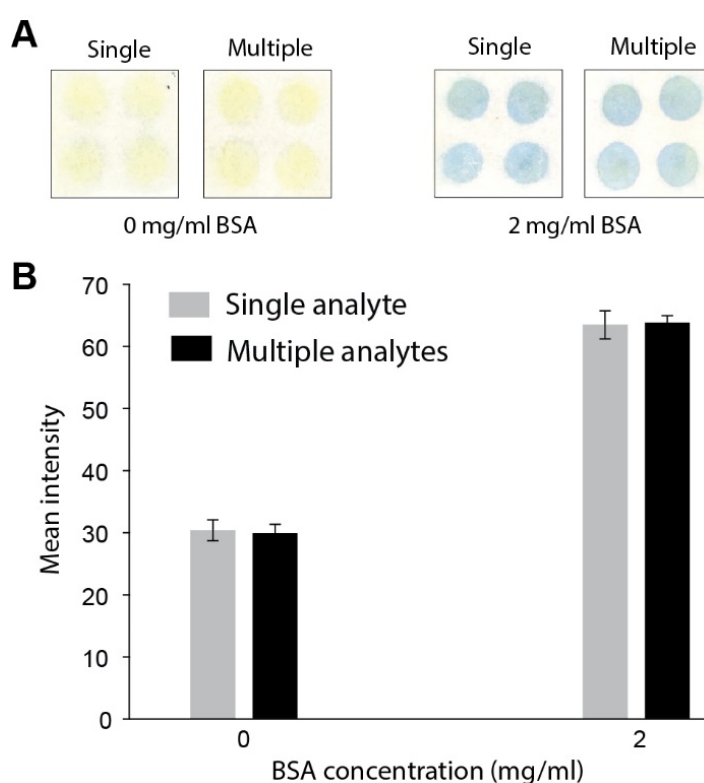

Figure S2. Uniform rehydration of 20 reagents. **(A)** End point image of an assembly consisting of 20 spots of Bromophenol blue dye post addition of 1M HCl. **(B)** Variation of signal intensity with position of spots for the end point image taken by smartphone and scanner. The final image intensity does not vary with location of spots and is similar for image taken using a smartphone (CV = 8.63%) and scanner (CV = 3.63%). N=3.

Uniformity of rehydrated spots over further higher number of spots was demonstrated using a sensitive bienzymatic assay of glucose detection. 32 spots of glucose chemistry, 0.4 ul each

were dried on 8 cm x 2cm paper assembly and 20 mg/dl dextrose solution was added as sample fluid (refer to SI video 2). On rehydration, 32 distinct pink signals were observed in 3 minutes which include time to fully develop colour. This is attributed to faster wicking rate of distribution layer which act as fluid source for detection layer having dried reagents.
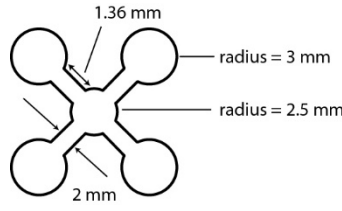
SI section 3. Effect of competing ions on signal intensity

BSA chemistry was selected to test specificity of assay by adding competing ions in sample fluid. Comparison was made by flowing 0 mg/ml BSA, i.e. DI water and 2 mg/ml BSA with and without the presence of interfering species: 20 mg/dl glucose, 0.5 mM SCN^-, 0.8 mM NO_2^- in sample fluid. No statistical difference in signal intensity was found when samples with and without interfering species were added for both 0 mg/ml and 2 mg/ml BSA (P>0.74).

Supporting figure 3. Investigation of interfering species in signal intensity. **(A)** Image of detection layer after rehydration with 0 mg/ml and 2 mg/ml BSA in the absence (single analyte) and presence (multiple analytes) of other analytes. **(B)** Bar graph comparing mean intensity at two different BSA concentration for image shown in **(A).** (N=4)

SI section 4. Comparison of signal intensity in BF-µPAD and µPAD

Supporting figure 4. Design of µPAD

Calculation of Limit of detection of protein assay performed on BF-µPAD and µPAD

Method for calculating LOD was directly adapted from Holstein et al.[3]

Step 1. Calculating L_C

Limit of detection (LOD) of assay in blank solution (Lc) is given by:

$$L_C = \mu_{blank} + t(1 - \alpha, n - 1)\sigma_{blank}$$

Where μ_{blank} and σ_{blank} are mean and standard deviation of n replicates of ban, α is probability of generating false positive results, and $t(1 - \alpha, n - 1)$ is $1 - \alpha$ percentile of t distribution at $(n - 1)$ degree of freedom.

Step 2. Calculating L_D

Limit of detection of assay in test solution (L_D) is given by:

$$L_D = L_C + t(1 - \beta, m(n - 1))\sigma_{test}$$

σ_{test} is pooled standard deviation of all test signals, calculated as:

$$\sigma_{test} = \sqrt{\frac{\sum_{i=1}^{m} \sigma_i^2}{m}}$$

m is number of test samples, β is probability of generating false positive signals, and $t(1 - \beta, m(n - 1))$ is $1 - \beta$ percentile of t distribution at $m(n - 1)$ degrees of freedom.

Step 3. Generating calibration curve between signal and concentration domain

Four parameters logistic (4PL) curve is used to translate the L_D value in the signal domain to an LOD estimate in the concentration domain in MATLAB using curve fitting toolbox. The equation is given by:

$$f(a, b, k, d, C) = S = \frac{a - d}{1 + \left(\frac{\log_{10}(C + 2)}{k}\right)^b} + d$$

S is signal intensity measured at C concentration of analyte. We define a matrix containing the fitted parameters, $\beta = (a, b, k, d)$.

Step 4. Calculating limit of detection in concentration domain

Inverting eq. (4) to make C as function of S and replacing S by L_D we get the LOD in concentration domain as:

$$y(a, b, k, d, L_D) = \log_{10}(LOD + 2) = k\left(\left(\frac{a - d}{L_D - d}\right) - 1\right)^{1/b}$$

Step 5. Calculating 95% confidence interval of limit of detection

To calculate 95% confidence interval, we need first calculate residual variance, given by:

$$\sigma^2 = \frac{sum\ of\ square\ error\ (SSE)}{n - p}$$

SSE is obtained from MATLAB curve fitting toolbox. p is number of parameters calculated, for 4PL curve, p = 4.

Next, we calculate variance-covariance Σ_β

$$\sum_{\beta} = inv\left[\frac{1}{\sigma^2}\left(\frac{\partial f}{\partial \beta}\right)' \times I(mn \times mn) \times \left(\frac{\partial f}{\partial \beta}\right)\right]$$

I is identity matrix. Using σ^2 and we calculate asymptotic variance as:

$$variance_{asym} = \frac{\sigma^2}{n}\left(\frac{\partial y}{\partial L_D}\right)^2 + \left(\frac{\partial y}{\partial \beta}\right)' \sum_{\beta} \left(\frac{\partial y}{\partial \beta}\right)$$

All partial derivatives and $variance_{asym}$ are calculated in MATLAB with the help of

MATLAB code provided by Holstein.

Standard error of LOD is given by $se = \sqrt{varaiance_{asym}}$

Finally, LOD 95% CI as [LOD$_{0.025}$, LOD$_{0.975}$] is calculates using the formula

$$\log_{10}(LOD_{0.025} + 2) = \log_{10}(LOD + 2) + z_{0.025}se$$

$$\log_{10}(LOD_{0.975} + 2) = \log_{10}(LOD + 2) + z_{0.075}se$$

$z_{0.025}$ and $z_{0.975}$ are lower 2.5th and 97.5th percentile of standard normal distribution.

parameter	BF-μPAD	μPAD
n	4	4
m	6	6
σ_{blank}	0.9523	0.9479
L_c	3.0306	3.0169
σ_{test}	1.6576	2.0536
L_D	6.5131	7.3314
$\beta = (a,b,k,d)$	(-84.23, 1.177, 0.3475, 100)	(-0.5166, 6.562, 0.6083, 87.41)
se	0.0055	0.0120
LOD	0.1816	0.6727
LOD 95% CI	(0.1283,0.2362)	(0.5314,0.8217)

Supporting table 2. Calculated and derived parameter for protein assay in BF-μPAD and

μPAD.

References:

(1)   Rath, D.; Sathishkumar, N.; Toley, B. J. Experimental Measurement of Parameters Governing Flow Rates and Partial Saturation in Paper-Based Microfluidic Devices. *Langmuir* **2018**, *34* (30), 8758–8766. https://doi.org/10.1021/acs.langmuir.8b01345.

(2)   Buser, J. R. Heat, Fluid, and Sample Control in Point -of-Care Diagnostics. *Univ. Washingt.* **2016**.

(3)   Holstein, C. A.; Griffin, M.; Hong, J.; Sampson, P. D. Statistical Method for Determining and Comparing Limits of Detection of Bioassays. *Anal. Chem.* **2015**, *87* (19), 9795–9801. https://doi.org/10.1021/acs.analchem.5b02082.